Theoretical Foundations of Chemical Engineering, Vol. 35, No. 1, 2001, pp. 28–38.
Translated from Teoreticheskie Osnovy Khimicheskoi Tekhnologii, Vol. 35, No. 1, 2001, pp. 31–41.

Laminar Heat Transfer in a Liquid Flowing in a Diverging Conical Annular Channel with a Varied Inner-Wall Temperature

L. M. Ul'ev

Kharkov State Polytechnical University, ul. Frunze 21, Kharkov, 310002 Ukraine

Received May 17, 1999

Abstract—The problem of convective heat transfer in a divergent slow liquid flow in a constant-width conical annular channel is analyzed for the case of first-kind thermal boundary conditions and linear variation of the inner-wall temperature along the channel length. The problem is solved by eigenfunction-series expansion. The spatial distribution of temperature is represented as the sum of two infinite series in confluent hypergeometric functions of the transverse coordinate that are multiplied by an exponential function of the axial coordinate and the angular opening of the cone. The solution is interesting in that it is the superposition of two solutions, each having its own eigenfunctions and eigenvalues.

In the extrusion of polymeric products such as strands, granules, tubes, and films, the molten polymer is forced through diverging channels formed by coaxial conical surfaces [1, 2]. To optimize the extruder design and process parameters, it is necessary to study the flow and heat transfer in extruder die channels. Present-day processes allow heat-transfer conditions to be varied at the channel walls, but experimental optimization of process parameters is rather expensive. In many cases, it is also unreasonable to numerically simulate polymer processing because the necessary relationships between process parameters can be established analytically. Below, known analytical solutions are used to develop numerical, asymptotic, and approximate calculation procedures.

Earlier [3, 4], we reported a solution to the problem of isothermic flow in conical annular channels with various wall arrangements. Laminar heat transfer in conical slits under third-kind boundary conditions was reported in [5]. In some cases, such as underwater granulation with a nonheated core, the temperature of one of the walls clearly varies along the channel. The temperature of the inner channel wall (inner conical surface) varies from the melt temperature at the die inlet to about the temperature of the water carrying the granules away. If the extruder core is heated, the inner-wall temperature at the channel inlet may exceed the melt temperature, and in the case of a heated bushing [6], it may increase along the channel. In the case of blow extrusion molding, the inner-wall temperature is governed by the temperature of the air fed into the extruder die.

To analyze the melt-temperature distribution, we will consider laminar heat transfer in conical annular channels under first-kind boundary conditions at a specified way of variation of the inner-wall temperature. We will deal with molten polymers that behave as Newtonian liquids under processing conditions [7]. It was demonstrated [5] that, for liquid flow rates and channel geometries important in practice, the Reynolds and Name–Griffith numbers are far less than unity ($\mathrm{Re} \ll 1$, $\mathrm{Gn} \ll 1$) and the Peclet number Pe is $\gg 100$. Therefore, polymer flows are typically creeping [8], heat dissipation can be disregarded, and the variation of the conductive heat flux is negligible as compared to the variation of the convective heat flux. In biconical coordinates (Fig. 1), which are defined as [9]

$$z' = R\cos\alpha + X\sin\alpha, \tag{1}$$

$$y' = (R\sin\alpha - X\cos\alpha)\sin\varphi, \tag{2}$$

$$x' = (R\sin\alpha - X\cos\alpha)\cos\varphi, \tag{3}$$

the set of axisymmetric heat-transfer equations will then appear as

$$\frac{\partial\Pi}{\partial\xi} = \frac{1}{\sigma}\frac{\partial}{\partial\chi}\left(\sigma\frac{\partial v}{\partial\chi}\right), \tag{4}$$

$$\frac{\partial\Pi}{\partial\chi} = \frac{\cos(\alpha)\sin(\alpha)}{\sigma^2}v, \tag{5}$$

$$\frac{\partial}{\partial\xi}(\sigma v) = 0, \tag{6}$$

$$\mathrm{Pe}_0 v\frac{\partial\Theta}{\partial\xi} = \frac{1}{\sigma}\frac{\partial}{\partial\chi}\left(\sigma\frac{\partial\Theta}{\partial\chi}\right), \tag{7}$$

where

$$\xi = R/h, \quad \chi = X/h,$$

$$V_0 = Q/[\pi h(2R_0\sin\alpha - h\cos\alpha)],$$

$$v = V_R/V_0, \quad \Pi = (P - P_0)h/(\gamma V_0),$$

0040-5795/01/3501-0028$25.00 © 2001 MAIK "Nauka/Interperiodica"

$$\sigma = \xi\sin\alpha - \chi\cos\alpha, \quad \mathrm{Pe}_0 = V_0 h/a,$$

$$\Theta = (T - T_0)/(T_1 - T_0).$$

The boundary and edge conditions for this problem are the following:

$$v = 0, \qquad \chi = 0, \quad \xi_0 < \xi \le \xi_1; \quad (8)$$

$$v = 0, \qquad \chi = 1, \quad \xi_0 < \xi \le \xi_1; \quad (9)$$

$$\Pi = 0, \qquad 0 \le \chi \le 1, \qquad \xi = \xi_0; \quad (10)$$

$$\Theta = 0, \qquad 0 \le \chi \le 1, \qquad \xi = \xi_0; \quad (11)$$

$$\Theta = 1, \qquad \chi = 0, \quad \xi_0 < \xi \le \xi_1; \quad (12)$$

$$\Theta = \Theta_2 + b(\xi - \xi_0), \qquad \chi = 1, \quad \xi_0 < \xi \le \xi_1. \quad (13)$$

Here,

$$b = \frac{T_3 - T_2}{(T_1 - T_0)\Delta\xi} < 1, \quad \Delta\xi = \xi_1 - \xi_0 = L/h.$$

In practice, $\xi\tan\alpha \gg 1$, and the solution to the set of Eqs. (4)–(6) and (8)–(10) is [3]

$$v = \frac{6(2\xi_0\sin\alpha - \cos\alpha)}{\cos\alpha - 2\xi\sin\alpha}(\chi^2 - \chi), \quad (14)$$

$$\Pi = -\frac{6(\cos\alpha - 2\xi_0\sin\alpha)}{\sin\alpha}\ln\frac{1 - 2\xi\tan\alpha}{1 - 2\xi_0\tan\alpha}. \quad (15)$$

Equation (7) will take the form

$$\frac{6\mathrm{Pe}_0(2\xi_0\sin\alpha - \cos\alpha)}{\cos\alpha - 2\xi\sin\alpha}(\chi^2 - \chi)\frac{\partial\Theta}{\partial\xi} = \frac{\partial^2\Theta}{\partial\chi^2}. \quad (16)$$

A solution to the problem ((16), (11)–(13)) will be sought for as the superposition of two solutions:

$$\Theta(\chi, t) = \Xi_1(\chi, t) + \Xi_2(\chi, t), \quad (17)$$

where $t = 2\chi - 1$; $\Xi_1(\xi, t)$ is the solution of Eq. (16) with the boundary conditions

$$\Xi_1 = \frac{1 + \Theta_2 + b(\xi - \xi_0)}{2}, \quad t = -1; \quad (18)$$

$$\Xi_1 = \frac{1 + \Theta_2 + b(\xi - \xi_0)}{2}, \quad t = 1; \quad (19)$$

$$\Xi_1 = 0, \quad \xi = \xi_0, \quad -1 < t < 1; \quad (20)$$

and $\Xi_2(\xi, t)$ is the solution of Eq. (16) for the boundary conditions

$$\Xi_2 = \frac{1 - \Theta_2 - b(\xi - \xi_0)}{2}, \quad t = -1; \quad (21)$$

$$\Xi_2 = \frac{-1 + \Theta_2 + b(\xi - \xi_0)}{2}, \quad t = 1; \quad (22)$$

$$\Xi_2 = 0, \quad \xi = \xi_0, \quad -1 < t < 1. \quad (23)$$

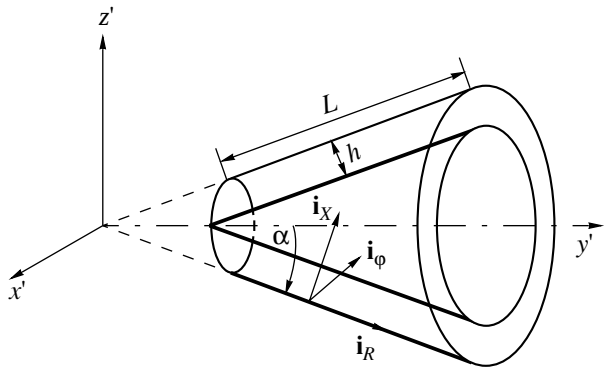

Fig. 1. Geometry of a conical channel of constant width. $\mathbf{i}_R$, $\mathbf{i}_X$, and $\mathbf{i}_\varphi$ are the unit vectors of the biconical coordinates.

To solve the problems ((16), (18)–(20)) and ((16), (21)–(23)), let us introduce new dependent variables:

$$\Xi_1(\xi, t) = \Phi_1(\xi, t) + \frac{1 + \Theta_2 + b(\xi - \xi_0)}{2}, \quad (24)$$

$$\Xi_2(\xi, t) = \Phi_2(\xi, t) + \frac{\Theta_2 - 1 + b(\xi - \xi_0)}{2}t, \quad (25)$$

The functions $\Phi_i(\xi, t)$ (hereafter, $i = 1, 2$) transform nonuniform boundary conditions (18), (19), (21), and (22) into uniform ones:

$$\Phi_i = 0, \quad \chi = 0, \quad t = -1; \quad (26)$$

$$\Phi_i = 0, \quad \chi = 1, \quad t = 1, \quad (27)$$

The conditions at the channel inlet, given by Eqs. (20) and (23), will take the form

$$\Phi_1(\xi_0, t) = -\frac{1 + \Theta_2}{2}, \quad (28)$$

$$\Phi_2(\xi_0, t) = \frac{1 - \Theta_2}{2}t. \quad (29)$$

Next, by substituting the $\Xi_i(\xi, t)$ functions into Eq. (16) and changing the variables, we obtain nonuniform equations in $\Phi_i(\xi, t)$:

$$\frac{8(\cos\alpha - 2\xi\sin\alpha)}{3\mathrm{Pe}(1 - t^2)}\frac{\partial^2\Phi_i}{\partial\xi} + \frac{\partial\Phi_i}{\partial t^2} + f_i(\xi, t) = 0, \quad (30)$$

where

$$\mathrm{Pe} = \mathrm{Pe} = Q/(\pi a h).$$

Then,

$$\mathrm{Pe}_0 = \frac{\mathrm{Pe}}{2\xi_0\sin\alpha - \cos\alpha},$$

and it follows from Eqs. (24) and (25) that

$$f_1(\xi, t) = b/2, \quad f_2(\xi, t) = bt/2.$$

Let us represent the solution of Eq. (30) as the product $\Phi_i(\xi, t) = Y_i(\xi)\Psi_i(\chi)$ (summation over i is not performed) and consider the uniform equation corresponding to Eq. (30). We will then arrive at the Sturm–Liouville problem stated by the set of equations

$$\Psi_i'' + \mu_i^2(1 - t^2)\Psi_i = 0, \tag{31}$$

$$\Psi_i = 0, \quad t = -1; \tag{32}$$

$$\Psi_i = 0, \quad t = 1, \tag{33}$$

Here, $\mu_i = \beta_i/4$ and β_i is the separation constant for the uniform equation (30).

It has been demonstrated [5] that Eq. (31) reduces to the Whittaker equation and that its solution is

$$\Psi(t) = C_1\sqrt{\mu}\exp\left(-\frac{\mu t^2}{2}\right){}_1F_1\left(\frac{3-\mu}{4}, \frac{3}{2}; \mu t^2\right) + C_2\exp\left(-\frac{\mu t^2}{2}\right){}_1F_1\left(\frac{1-\mu}{4}, \frac{1}{2}; \mu t^2\right), \tag{34}$$

where ${}_1F_1(\alpha, \gamma; x)$ is a degenerate hypergeometric function and C_1 and C_2 are arbitrary constants.

By substituting Eq. (34) into Eqs. (32) and (33), we obtain

$$-C_1\sqrt{\mu}\exp\left(-\frac{\mu}{2}\right){}_1F_1\left(\frac{3-\mu}{4}, \frac{3}{2}; \mu\right) + C_2\sqrt{\mu}\exp\left(-\frac{\mu}{2}\right){}_1F_1\left(\frac{1-\mu}{4}, \frac{1}{2}; \mu\right) = 0, \tag{35}$$

$$C_1\sqrt{\mu}\exp\left(-\frac{\mu}{2}\right){}_1F_1\left(\frac{3-\mu}{4}, \frac{3}{2}; \mu\right) + C_2\sqrt{\mu}\exp\left(-\frac{\mu}{2}\right){}_1F_1\left(\frac{1-\mu}{4}, \frac{1}{2}; \mu\right) = 0. \tag{36}$$

Obviously, Eqs. (35) and (36) are simultaneous only when $C_1 = 0$ or $C_2 = 0$. In the former case, the equation for eigenvalues is

$${}_1F_1\left(\frac{1-\mu}{4}, \frac{1}{2}; \mu\right) = 0 \tag{37}$$

and the eigenfunctions are expressed as

$$\Psi_{1n} = C\exp\left(-\frac{\mu_{1n}t^2}{2}\right){}_1F_1\left(\frac{1-\mu_{1n}}{4}, \frac{1}{2}; \mu_{1n}t^2\right). \tag{38}$$

At $C_2 = 0$, the eigenvalues are determined from the equation

$${}_1F_1\left(\frac{3-\mu}{4}, \frac{3}{2}; \mu\right) = 0, \tag{39}$$

and the eigenfunctions are expressed as

$$\Psi_{2n} = C\sqrt{\mu_{2n}}\exp\left(-\frac{\mu_{2n}t^2}{2}\right)t{}_1F_1\left(\frac{3-\mu_{2n}}{4}, \frac{3}{2}; \mu_{2n}t^2\right). \tag{40}$$

Note that the μ_n value can be calculated, to an acceptable accuracy, from the relationship $\mu_{1n} = 4n + 5/3$ [10], and calculations for $n > 4$, demonstrated the validity of the equality $\mu_{2n} = \mu_{1n} + 2$.

With the use of Eqs. (31)–(33), it is easy to prove that the sets of functions defined by Eqs. (38) and (40) are orthogonal and $(1 - t^2)$-weighted in the interval [–1, 1]. Therefore, the source term in Eq. (30) can be represented as an expansion in the eigenvectors of problem (31)–(33):

$$f_i(\xi, t) = \sum_{n=1}^{\infty} f_{in}(\xi)\Psi_{in}. \tag{41}$$

The orthogonality of eigenfunctions enables us to determine the expansion coefficients:

$$f_{in} = \left(\int_{-1}^{1}(1 - t^2)f_i(\xi, t)\Psi_{in}(t)dt\right)/\|\Psi_{in}\|^2, \tag{42}$$

where

$$\|\Psi_{in}\|^2 = \int_{-1}^{1}(1 - t^2)\Psi_{in}^2 dt$$

is the squared norm of the eigenfunctions.

The function $(1 - t^2)$ is even in the interval [–1, 1], and $f_1(\xi)$ is independent of t. If the functions defined by Eqs. (39) and (40), which are odd in the interval [–1, 1], are selected as the basis for solving the problem ((16), (18)–(20)), then the $f_{1n}(\xi)$ coefficients will all be zero. Therefore, the set of functions defined by Eqs. (37) and (38) should be taken as the orthogonal basis.

Similarly, in solving the problem ((16), (21)–(23)), for which the function $f_{2n}(\xi, t)$ is odd in the interval [–1, 1], the basis will be the set of odd functions defined by Eqs. (39) and (40).

Equation (42) can then be rewritten as

$$f_{1n} = \frac{b}{2}\frac{\int_{-1}^{1}(1 - t^2)\Psi_{1n}(t)dt}{\|\Psi_{1n}\|^2} = \frac{b}{2}M_n, \tag{43}$$

$$f_{2n} = \frac{b}{2}\frac{\int_{-1}^{1}t(1 - t^2)\Psi_{2n}(t)dt}{\|\Psi_{2n}\|^2} = \frac{b}{2}K_n, \tag{44}$$

Thus, we have derived the eigenfunctions for the problems to be solved. The general solutions to the

problems ((16), (18)–(20)) and ((16), (21)–(23)) are the sums of the respective particular solutions:

$$\Phi_1(\xi, t) = \sum_{n=1}^{\infty} Y_{1n}(\xi) \times \exp\left(-\frac{\mu_{1n} t^2}{2}\right) {}_1F_1\left(\frac{1-\mu_{1n}}{2}, \frac{1}{2}; \mu_{1n} t^2\right), \quad (45)$$

$$\Phi_2(\xi, t) = \sum_{n=1}^{\infty} Y_{2n}(\xi) \times \exp\left(-\frac{\mu_{2n} t^2}{2}\right) t\, {}_1F_1\left(\frac{3-\mu_{2n}}{2}, \frac{3}{2}; \mu_{2n} t^2\right). \quad (46)$$

By substituting the Φ_i functions and expansions (43) and (44) into Eq. (30) and its initial conditions, we obtain a set of ordinary differential equations for determining the $Y_{in}(\xi)$ functions:

$$Y'_{in} - \frac{8\mu_i^2}{3\mathrm{Pe}}(\cos\alpha - 2\xi\sin\alpha) Y_{in} + f_{in} = 0, \quad (47)$$

$$Y_{in}(\xi_0) = \left(\int_{-1}^{1} \Phi_i(\xi_0, t)(1-t^2)\Psi_{in}(t)\,dt\right) / \|\Psi_{in}\|^2. \quad (48)$$

Equations (47) and (48) can be solved by the method of variation of the arbitrary constant:

$$Y_{1n}(\xi) = -\frac{M_n}{2}\left\langle \frac{1+\Theta_2}{2} \times \exp\left\{\frac{8\mu_{1n}^2(\xi-\xi_0)[\cos\alpha - (\xi+\xi_0)\sin\alpha]}{3\mathrm{Pe}}\right\} + \frac{b}{6\mathrm{Pe}} I_{1n}\right\rangle, \quad (49)$$

$$Y_{2n}(\xi) = \frac{K_n}{2}\left\langle \frac{1-\Theta_2}{2} \times \exp\left\{\frac{8\mu_{2n}^2(\xi-\xi_0)[\cos\alpha - (\xi+\xi_0)\sin\alpha]}{3\mathrm{Pe}}\right\} + \frac{b}{6\mathrm{Pe}} I_{2n}\right\rangle. \quad (50)$$

where

$$I_{in} = \int_{\xi_0}^{\xi} (\cos\alpha - 2\tau\sin\alpha) \times \exp\left\{\frac{8\mu_{in}^2(\xi-\xi_0)[\cos\alpha - (\xi+\tau)\sin\alpha]}{3\mathrm{Pe}}\right\} d\tau. \quad (51)$$

The solution of the problem in terms of the original variables will appear as

$$\Theta(\xi, \chi) = 1 + [\Theta_2 - 1 + b(\xi - \xi_0)]\chi + \Phi_1(\xi, \chi) + \Phi_2(\xi, \chi), \quad (52)$$

It enables us to derive an expression for the average flow-bulk temperature:

$$\bar{\Theta} = \frac{2\pi\int_0^1 v\Theta(\xi, \chi)(\xi\sin\alpha - \chi\cos\alpha)\,d\chi}{\bar{v}\pi(2\xi\sin\alpha - \cos\alpha)} = \frac{12}{\cos\alpha - 2\xi\sin\alpha}\int_0^1 (\chi^2 - \chi)\Theta(\xi\sin\alpha - \chi\cos\alpha)\,d\chi, \quad (53)$$

where

$$\bar{v} = \frac{2\xi_0\sin\alpha - \cos\alpha}{2\xi\sin\alpha - \cos\alpha} \quad (54)$$

is the average dimensionless velocity.

The dimensionless local heat flux or, in other terms, the Nusselt number at a channel wall is conventionally defined as the ratio of the convective heat-transfer coefficient to the difference between the average flow-bulk temperature and the wall temperature:

$$\mathrm{Nu}_1 = \frac{\alpha_1 h}{\lambda} = \frac{\partial\Theta/\partial\chi|_{\chi=0}}{\bar{\Theta} - \Theta|_{\chi=0}}, \quad \mathrm{Nu}_2 = \frac{\alpha_2 h}{\lambda} = \frac{\partial\Theta/\partial\chi|_{\chi=1}}{\bar{\Theta} - \Theta|_{\chi=1}}. \quad (55)$$

When so defined, Nu_i may have discontinuities at ξ values for which the weight-average temperature is equal to the temperature of a wall. This may also be the case if Nu is defined as the ratio of the convective heat-transfer coefficient to the difference between the average flow-bulk temperature and the average (initial or current) wall temperature. For this reason, we now introduce the dimensionless convective heat-transfer coefficient as the ratio of the heat flux at a channel wall to the scaling temperature

$$\mathrm{Nu}^* = -\left.\frac{\partial\Theta}{\partial\mathbf{n}}\right|_{\mathbf{n}=0}, \quad (56)$$

where **n** is the normal directed toward the liquid. We then arrive at the following expressions for the dimensionless heat fluxes at the channel walls:

$$\mathrm{Nu}_1^* = -\left.\frac{\partial\Theta}{\partial\chi}\right|_{\chi=0}, \quad \mathrm{Nu}_2^* = \left.\frac{\partial\Theta}{\partial\chi}\right|_{\chi=1}. \quad (57)$$

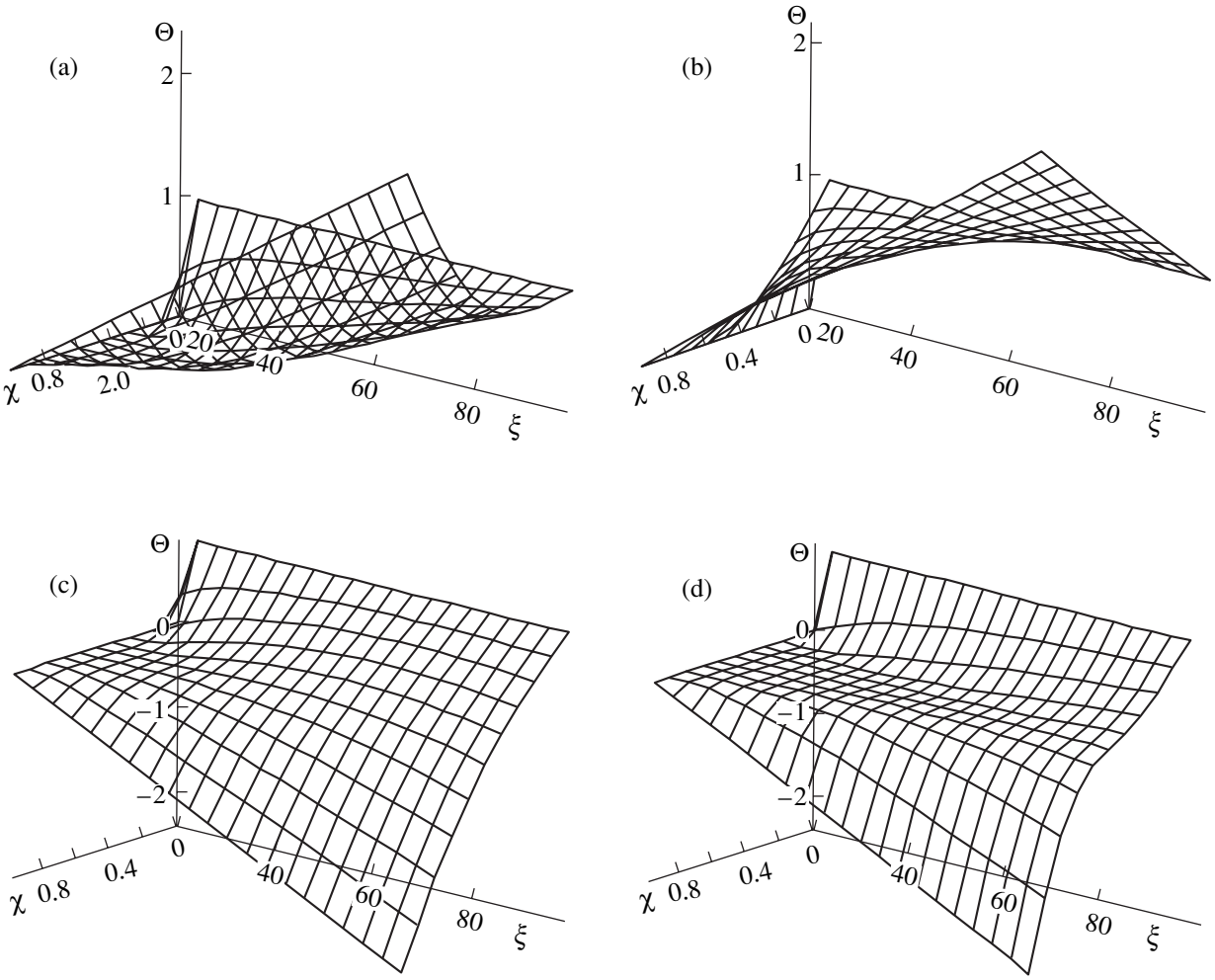

Fig. 2. Distribution of Θ in the channel at $\xi_0 = 20$ and $\xi_1 = 100$: (a) $\alpha = 15°$, $Pe = 10^4$, $\Theta_2 = 0$, and $b = 0.03$; (b) $\alpha = 90°$, $Pe = 2 \times 10^3$, $\Theta_2 = 0$, and $b = 0.03$; (c) $\alpha = 60°$, $Pe = 2 \times 10^4$, $\Theta_2 = 0$, and $b = -0.03$; (d) $\alpha = 5°$, $Pe = 2 \times 10^4$, $\Theta_2 = 0$, and $b = -0.03$.

By performing differentiation in Eqs. (57), we obtain

$$\left.\frac{\partial\Theta}{\partial\chi}\right|_{\chi=0} = \Theta_2 - 1 + b(\xi - \xi_0) + \sum_{n=1}^{\infty} Y_{1n}\Psi'_{1n}\Big|_{\chi=0} + \sum_{n=1}^{\infty} Y_{2n}\Psi'_{2n}\Big|_{\chi=0}, \quad (58)$$

$$\left.\frac{\partial\Theta}{\partial\chi}\right|_{\chi=1} = \Theta_2 - 1 + b(\xi - \xi_0) + \sum_{n=1}^{\infty} Y_{1n}\Psi'_{1n}\Big|_{\chi=1} + \sum_{n=1}^{\infty} Y_{2n}\Psi'_{2n}\Big|_{\chi=1}, \quad (59)$$

where

$$\Psi'_{1n}\Big|_{\chi=0} = -\Psi'_{1n}\Big|_{\chi=1} = -2\mu_{1n}(1-\mu_{1n})\exp\left(-\frac{\mu_{1n}}{2}\right){}_1F_1\left(\frac{5-\mu_{1n}}{4}, \frac{3}{2}; \mu_{1n}\right),$$

$$\Psi'_{2n}\Big|_{\chi=0} = \Psi'_{2n}\Big|_{\chi=1} = \frac{2\sqrt{\mu_{2n}}\mu_{2n}(3-\mu_{2n})}{3}\exp\left(-\frac{\mu_{2n}}{2}\right){}_1F_1\left(\frac{7-\mu_{2n}}{4}, \frac{5}{2}; \mu_{2n}\right).$$

Since Eqs. (57) are completely defined by the derivatives of temperature, we will use Eqs. (58) and (59) in the analysis of heat fluxes at the channel walls.

The parameters defining a solution to the problem are the Peclet number Pe; the inner-wall dimensionless temperature at the channel inlet, Θ_2; the dimensionless inlet coordinate ξ_0; angular opening of the cone, 2α; and the parameter b, which defines the distribution of the inner-wall temperature (temperature of the $\chi = 0$ boundary) over the channel length.

The solution at $b > 0$ and $\Theta_2 = 0$ describes heat transfer in the case that the inner-wall temperature T_2 is equal to the inlet liquid temperature T_0 and, if $T_1 < T_0$, decreases along the channel to some temperature $T_3 < T_2$ or, if $T_1 > T_0$, increases to a $T_3 > T_2$. The former sit-

uation can be observed in a submerged granulator with nonheated core and bushing. The latter situation sometimes occurs in the blow extrusion of polymeric films and in the underwater granulation with an externally heated distributing section and heated die channels [6].

The solution at $b < 0$ and $\Theta_2 = 0$ corresponds to the case that the outer-wall temperature is lower than the flow temperature at the channel inlet, $T_1 < T_0$, and the inner-wall temperature varies from T_0 to $T_3 > T_2$. This situation can be observed in the distributing section of a submerged granulator with a heated bushing and a nonheated body. At $T_1 > T_0$, we deal with a heated body and a nonheated bushing.

At $b > 0$ and $\Theta_2 = 0$, the thermal boundary layer is more extensive at the outer than at the inner channel wall (Fig. 2). Nu_1^* reaches its maximum at the outer wall, but it falls as the temperature field develops (Fig. 3). The Nu_2^* value at the inner channel wall near the inlet is close to zero and increases with changing inner-wall temperature (Fig. 3). For the Peclet number and boundary conditions considered, the average flow-bulk temperature monotonically grows along the channel, remaining below the inner-wall temperature (Fig. 4).

Decreasing Pe raises the contribution of heat conduction to heat transfer and shortens the length of the thermal boundary layer at the inlet (Fig. 2b). The dimensionless heat flux at the outer channel wall, Nu_1^*, falls sharply as the thermal boundary layer spreads along the channel and, at some distance from the inlet, changes its sign (Fig. 3). This behavior of Nu_1^* is explained by the fact that, at this point, the dimensionless flow temperature transcends the outer-wall temperature throughout the cross section owing to the heat influx from the inner wall, whose dimensionless temperature increases along the channel (Fig. 2).

The heat flux at the inner wall, Nu_2^*, somewhat rises along the channel because of the increase in the inner-wall temperature. However, since the inlet dimensionless temperature of the outer@wall is higher than that of the inner wall, and the thermal boundary layer at the Pe values considered spreads rapidly throughout the channel cross section, the dimensionless temperature of the flow near the inner wall transcends the dimensionless wall temperature at some point, and Nu_2^* changes its sign. If the liquid is heated from the outer wall, then, at this point, it begins to cool at the inner wall, and vice versa. In going downstream, the inner-wall dimensionless temperature becomes, at some point, higher than the dimensionless temperature of the adjacent liquid layer, and the heat flux changes its direction again (Fig. 3). Starting at this point, the distribution of temperature is essentially linear in any channel cross section (Fig. 2); that is, as ξ increases, only the linear term in expansions (58) and (59) remains signif-

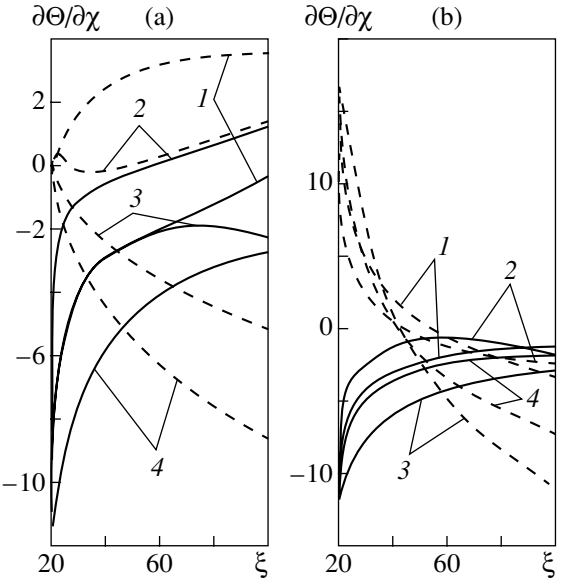

Fig. 3. Distribution of $\partial\Theta/\partial\chi$ at $\chi = 0$ (solid lines) and $\chi = 1$ (dashed lines): (a) $\Theta_2 = 0$; Pe = (*1*, *4*) 10^4, (*2*) 2×10^3, and (*3*) 2×10^4; α = (*1*) 15°, (*2*) 90°, (*3*) 60°, and (*4*) 5°; b = (*1*, *2*) 0.03 and (*3*, *4*) –0.03; (b) $\Theta_2 = 1.5$; Pe = (*1*, *2*) 10^4 and (*3*, *4*) 7×10^4; α = (*1*, *3*) 15° and (*2*, *4*) 90°; b = (*1*, *2*) –0.03 and (*3*, *4*) –0.05.

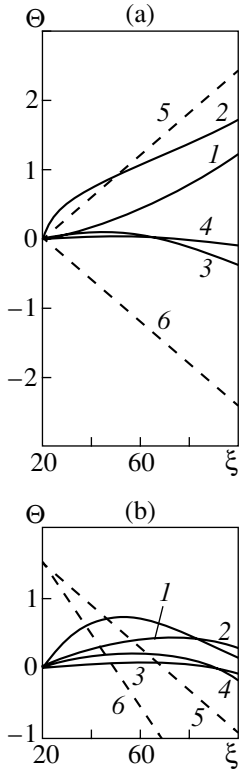

Fig. 4. Distribution of Θ in the channel: (a) $\Theta_2 = 0$; Pe = (*1*, *4*) 10^4, (*2*) 2×10^3, and (*3*) 2×10^4; α = (*1*) 15°, (*2*) 90°, (*3*) 60°, and (*4*) 5°; b = (*1*, *2*) 0.03 and (*3*, *4*) –0.03; lines *5* and *6* represent the dimensionless temperature of the inner channel wall ($\chi = 1$) at b = 0.03 and –0.03, respectively; (b) $\Theta_2 = 1.5$; Pe = (*1*, *2*) 10^4 and (*3*, *4*) 7×10^4; α = (*1*, *3*) 15° and (*2*, *4*) 90°; b = (*1*, *2*) –0.03 and (*3*, *4*) –0.05; lines *5* and *6* represent the dimensionless temperature of the inner wall ([chi] = 1) at b = –0.03 and –0.05, respectively.

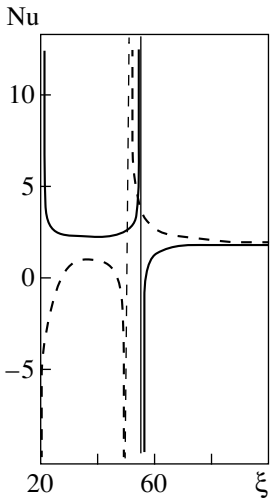

Fig. 5. Axial distribution of Nu_1 (solid lines) and Nu@2 (dashed lines) at $Pe = 2 \times 10^3$, $\alpha = 90°$, $b = 0.03$, and $\Theta_2 = 0$.

icant. Therefore, we can write the following expression for the limiting Nu_1^* and Nu_2^* values:

$$Nu_{1\infty}^* = -Nu_{2\infty}^* = \Theta_2 - 1 + b(\xi - \xi_0). \qquad (60)$$

At the channel inlet, the liquid flow gains more heat from the outer wall than it transfers to the inner wall, and, as a consequence, the average flow-bulk temperature is higher than the inner-wall temperature. However, because the inner-wall dimensionless temperature decreases along the channel, the temperatures become equal at some distance from the inlet. Downstream of this point, the flow temperature varies only owing to heat exchange with the inner wall, whose dimensionless temperature exceeds both the average flow-bulk and the outer-wall dimensionless temperatures, and as a consequence, the former is higher than the latter (Fig. 4).

At the points where the average flow-bulk temperature is equal to a wall temperature, the variation of the conventionally defined Nusselt numbers (see Eq. (55))

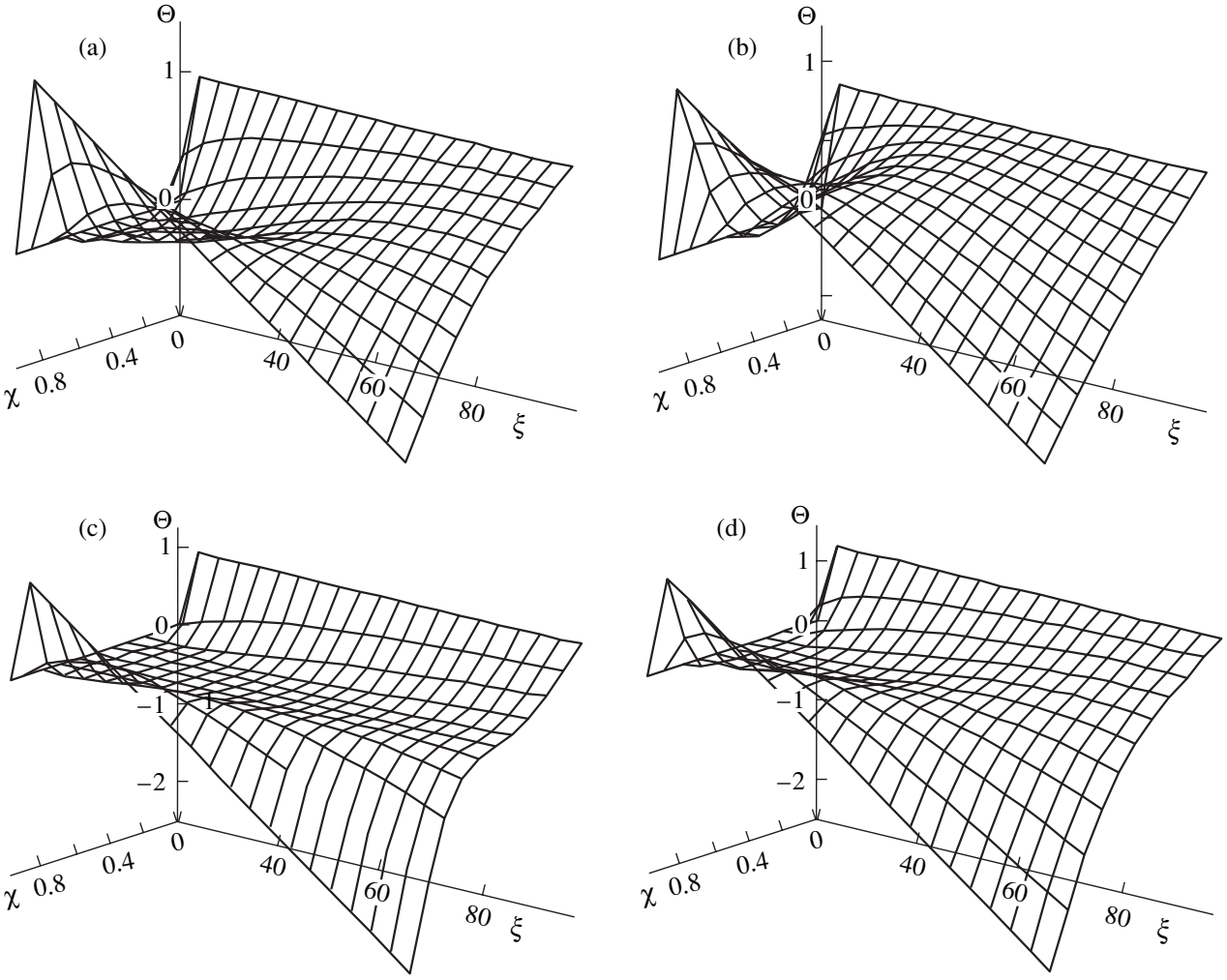

Fig. 6. Distribution of Θ in the channel at $\xi_0 = 20$, $\xi_1 = 100$, $\Theta_2 = 1.5$, α = (a, c) 15° and (b, d) 90°, Pe = (a, b) 10^4 and (c, d) 7×10^4, and b = (a, b) –0.03 and (c, d) –0.05.

with ξ shows discontinuities (Fig. 5), although no peculiarities are observed in the temperature distribution. It is, therefore, reasonable to use Eq. (57) for the dimensionless heat flux in the analysis of convective heat transfer in channels whose cross section is a multiply connected region. Nevertheless, in going downstream, Nu_1 and Nu_2 tend to their limiting value $Nu_{1\infty} = Nu_{2\infty} = 2$ (Fig. 5). Note that Nu_1 and Nu_2 tend to 2 from below and above, respectively, for all of the heat-transfer variants examined.

The existence of the limiting Nusselt numbers suggests that, as the

$$8(\xi - \xi_0)[\cos\alpha - (\xi + \xi_0)\sin\alpha]/(3\mathrm{Pe})$$

parameter, and the ξ value in particular, increase, the heat flux at a channel wall varies as the difference between the wall temperature and the average flow-bulk temperature. This is evidence of heat transfer stabilization. From Eqs. (53) and (58) and the Nu_∞ values, we obtain the following expression for steady-state heat transfer:

$$\bar{\Theta}_\infty = \frac{1 + \Theta_2}{2} + \frac{b}{2}(\xi - \xi_0). \qquad (61)$$

Let us turn to the heat transfer at $b < 0$, $\xi_0 = 20$, $\xi_1 = 100$, $\Theta_2 = 0$, $\mathrm{Pe} = 2 \times 10^4$, and $\alpha = 60°$.

In this case, the dimensionless liquid temperature increases at the outer wall to a greater extent than it decreases at the inner wall. As a consequence, the average flow-bulk temperature somewhat increases at the inlet but then falls along the channel because of decreasing inner-wall dimensionless temperature (Fig. 4).

The heat flux at the outer channel wall, Nu_1^*, is a nonmonotonic function of the axial coordinate. It first grows because of the developing thermal boundary layer to attain its minimum and then, provided that the temperature distribution in the channel is linear, begins to grow according to Eq. (60). The heat flux at the inner wall, Nu_2^*, monotonically increases owing to the wall-temperature variation (Fig. 3).

At $\alpha = 5°$ and the same values of the other parameters, the thermal boundary layer has no time to extend throughout the channel cross section because of the increased liquid flow rate, which grows hyperbolically with decreasing α (see Eq. (54)), and the reduced heat-transfer surface area. As a consequence, Nu_1^* grows monotonically and Nu_2^* diminishes along the channel (Fig. 3). The average flow-bulk temperature varies little (Fig. 3). The solution for $\Theta_2 < 0$, $b < 0$, and $T_1 < T_0$ applies to the case that the core tip is cooled below T_0 and the core-surface temperature grows along the channel length. At $T_1 > T_0$, the core-tip temperature is above the melt temperature and the core-surface temperature decreases along the channel length.

When $\mathrm{Pe} = 10^4$, $\Theta_2 = 1.5$, $b = -0.03$, $\xi_0 = 20$, and $\alpha = 15°$, the liquid flows within the initial thermal region, as indicated by both the unsteady temperature distribution (Fig. 6) and the variation of heat fluxes at the walls (Fig. 3b). Near the inlet, the dimensionless temperature increases almost equally at the inner and the outer wall. However, in going along the channel, the dimensionless temperature of the thermal boundary layer at the inner wall decreases to become negative, following the inner-wall dimensionless temperature. The radial distribution of temperature tends to linearity, but, for the set of parameters considered, heat transfer remains unsteady within the channel (Fig. 6). Because of such distribution of local temperature, the average flow-bulk temperature varies nonmonotonically (Fig. 4b).

As demonstrated above, raising α to 90° with the other parameters held constant reduces the average flow velocity and increases the heat-transfer surface area. As a result, the liquid stays in the channel for a shorter time and the thermal wall layers spread over the entire channel cross section at a shorter distance from the inlet (Fig. 6b). In this case, the maximum value of the average flow-bulk dimensionless temperature is higher than that at $\alpha = 15°$ (Fig. 4b), and both the axial and transverse distributions of temperature become linear within the channel. Therefore, the dimensionless heat fluxes at the walls are described by the linear limiting relationships (60) (Fig. 3b).

Raising Pe to 7×10^4 increases the contribution from convection to the heat transfer, and the initial thermal region is lengthened as a result. The inner-wall thermal boundary layer has no time to extend into the flow bulk even if the inner-wall temperature varies more considerably than in the previous cases (Fig. 6c). The flow-bulk dimensionless temperature varies little within the channel (Fig. 4b), and the dimensionless heat fluxes do not attain their limiting values (Fig. 3b). At $\alpha = 90°$, the thermal layer extends throughout the channel cross section (Fig. 6d). The temperature variation range is twice as wide as in the previous case (Fig. 4b), but the heat fluxes at the walls do not reach their limiting values (Fig. 3b).

The solution for $\Theta_2 < 0$ and $b > 0$ applies to two cases: (1) the outer-wall temperature is maintained below T_0, and the inner-wall temperature T_2, initially above T_0, decreases along the channel; (2) the outer-wall temperature is above T_0, and the inner-wall temperature T_2, initially below T_0, grows along the channel.

For $\mathrm{Pe} = 2 \times 10^4$, $\Theta_2 = -1.5$, $b = 0.05$, $\alpha = 15°$, $\xi_0 = 20$, and $\Delta\xi = 80$, the dimensionless liquid temperature increases near the outer wall ($\chi = 0$) and decreases near the inner wall ($\chi = 1$) (Fig. 7a). Since the absolute value of the inner-wall dimensionless temperature at the inlet is greater than unity, the average flow-bulk dimensionless temperature slightly decreases near the inlet (Fig. 8a). The greatest wall heat fluxes are observed there

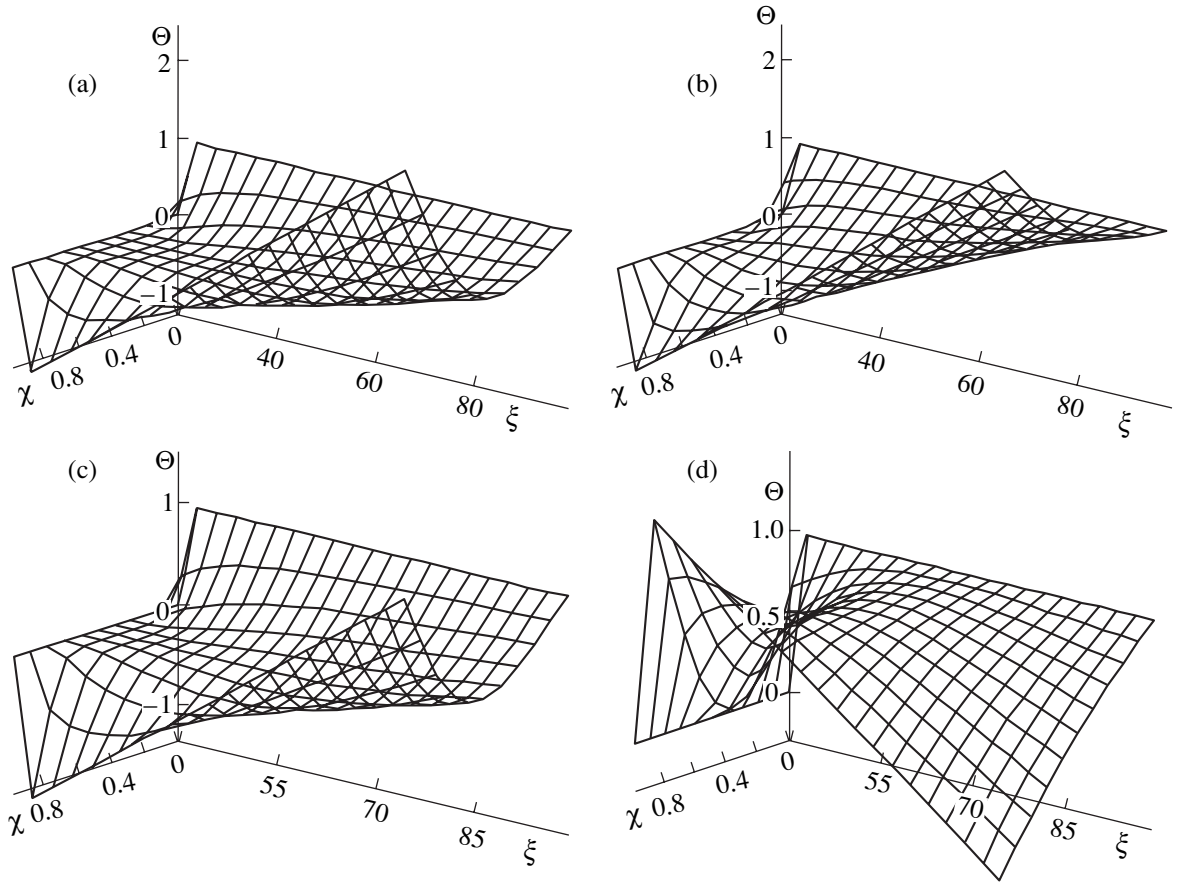

Fig. 7. Distribution of Θ in the channel at ξ_0 = (a, b) 20 and (c, d) 40, ξ_1 = (a–d) 100, Θ_2 = (a–d) 1.5, α = (a, c, d) 15° and (b) 90°, Pe = (a–c) 2×10^4 and (d) 2×10^3, and b = (a–c) 0.05 and (d) –0.03.

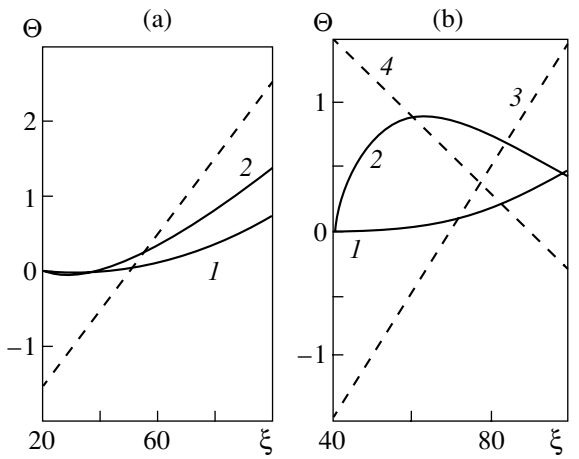

Fig. 8. Axial distribution of the average flow-bulk (solid lines) and inner-wall (dashed lines) dimensionless temperatures: (a) ξ_0 = 20, Pe = (*1*, *2*) 2×10^4, α = (*1*) 15° and (*2*) 90°, b = (*1*, *2*) 0.05, and Θ_2 = (*1*, *2*) –1.5; (b) ξ_0 = 40, Pe = (*1*) 2×10^4 and (*2*) 2×10^3, α = (*1*, *2*) 15°, b = (*1*, *3*) 0.05 and (*2*, *4*) –0.03, and Θ_2 = (*1*) –1.5 and (*2*) 1.5.

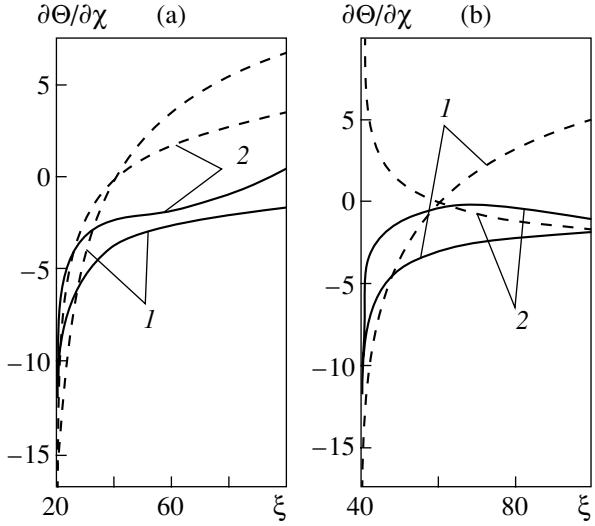

Fig. 9. Distribution of $\partial\Theta/\partial\chi$ at the χ = 0 (solid lines) and χ = 1 (dashed lines) channel walls: (a) ξ_0 = 20, Pe = (*1*, *2*) 2×10^4, α = (*1*) 15° and (*2*) 90°, b = (*1*, *2*) 0.05, and Θ_2 = (*1*, *2*) –1.5; (b) ξ_0 = 40, Pe = (*1*) 2×10^4 and (*2*) 2×10^3, α = (*1*, *2*) 15°, b = (*1*) 0.05 and (*2*) –0.03, and Θ_2 = (*1*) –1.5 and (*2*) 1.5.

(Fig. 9a). In going downstream, the inner-wall dimensionless temperature grows and, at some distance from the inlet, transcends the temperature of the adjacent liquid layer, and the inner-wall heat flux changes its sign (Fig. 9a). The average flow-bulk dimensionless temperature grows uniformly with increasing inner-wall dimensionless temperature (Fig. 8a), but heat transfer does not stabilize within the channel.

At a larger α, the thermal boundary layer will extend throughout the channel cross section at a shorter distance from the inlet. The dimensionless temperature of the flow will differ from those of the walls by a lesser value than it does in the previous case, giving rise to lower heat fluxes at the walls (Fig. 9a). The heat flux will change its direction at both walls (Fig. 9a). At the inner wall, it will do so because, at some point, the dimensionless wall temperature becomes higher than that of the arriving liquid, and at the outer wall, because the dimensionless temperature of the flowing liquid, which exchanges heat with the inner wall, becomes higher than the outer-wall temperature.

The heat transfer is also strongly dependent on the channel-inlet coordinate ξ_0. Raising ξ_0 at a fixed α causes an increases in the cross-sectional area of the channel and in the heat-transfer area. Therefore, at a constant Pe value, the thermal boundary layer will occupy the entire cross section at a shorter distance from the inlet (Fig. 7c). The behaviors of the average flow-bulk dimensionless temperature and the heat fluxes will remain essentially unchanged (Figs. 8b, 9b).

Simultaneously reducing Pe and raising ξ_0 will result in a developed temperature field at a short distance from the inlet. This is clearly seen in the case of $\mathrm{Pe} = 2 \times 10^3$, $\Theta = 1.5$, $b = -0.03$, $\alpha = 15°$, and $\xi_0 = 40$ (Fig. 7d; see also Fig. 6a). In this case, the distributions of the average flow-bulk dimensionless temperature and wall heat fluxes in the channel are described by limiting relationships (Figs. 8b, 9b).

Note that the functional series (45) and (46) are uniformly convergent for $\xi > \xi_0$ at any problem parameters satisfying the imposed constraints [11]. An analysis of Eqs. (49)–(51) and the numerical summation of series (45), (46), (58), and (59) demonstrates that, when the eigenvalues μ_{in} and the degenerate hypergeometric functions are determined with a relative error of 10^{-16}, the terms of the functional sequences of the partial sums of the series considered differ from each other by no more than 0.01 starting at $n \approx \mathrm{INT}[\sqrt{\mathrm{Pe}}/(\xi - \xi_0)^2]$. Series (45), (46), (58), and (59) were summed with precisely this relative error. The calculation accuracy can be checked using the energy conservation law

$$c\rho Q(\Delta\bar{T} - T_0) = 2\pi\int_{R_0}^{R_1}[(q_1 - q_2)R\sin\alpha + hq_2\cos\alpha]dR, \quad (62)$$

where q_1 and q_2 are the heat fluxes at $\chi = 0$ and 1, respectively. In the dimensionless form, Eq. (62) will appear as

$$\mathrm{Pe}\bar{\Theta} = 2\left\{\int_{\xi_0}^{\xi}\left[\xi\left(\left.\frac{\partial\Theta}{\partial\chi}\right|_{\chi=1} - \left.\frac{\partial\Theta}{\partial\chi}\right|_{\chi=0}\right)\sin\alpha - \left.\frac{\partial\Theta}{\partial\chi}\right|_{\chi=1}\cos\alpha\right]d\xi\right\}. \quad (63)$$

Calculations demonstrate that the right and the left of Eq. (63) coincide to a calculation accuracy.

NOTATION

a—thermal diffusivity, m^2/s;

b—coefficient defining the linear variation of the inner-wall temperature;

c—specific heat, J/(kg K);

h—channel width, m;

L—length of the cone generator, m;

P, P_0—current and inlet pressures, respectively, Pa;

Q—flow rate, m^3/s;

R, R_0, R_1—radial coordinate, m;

T, T_0—current and inlet temperatures, respectively, K;

T_1—temperature of the outer conical surface, K;

T_2, T_3—temperature of the inner conical surface at the channel inlet and outlet, respectively, K;

V, V_0—current and inlet flow velocities, respectively, m/s;

X—lateral biconical coordinate, m;

x', y', z'—Cartesian coordinates, m;

α—half the angular opening of the cone, deg;

α_1, α_2, – коэффициент теплоотдачи на границе $\chi = 0$, $\chi = 1$ соответственно, Вт/(м^2 K);

β—separation constant;

λ—heat conductivity of the liquid, W/(m K);

ν—dynamic viscosity, Pa s;

ρ—density, kg/m^3;

$\mathrm{Gn} = \nu V_0^2/(\lambda\Delta T_{\mathrm{rheol}})$—Name–Griffith number;

$\mathrm{Pe}_0 = V_0 hc\rho/\lambda$—Peclet number at the channel inlet;

$\mathrm{Re} = hV_0\rho/\nu$—Reynolds number.

INT – функция усечения.

REFERENCES

1. Joshi, M.V., *Dies for Plastics Extrusion*, Delhi: Macmillan, 1984, p. 176.
2. Sors, L., Bardocz, L., and Radnoti, I., *Plastic Molds and Dies*, Budapest: Akad. Kiado, 1980, p. 495.
3. Ul'ev, L.M., Slow Flow between Coaxial Conical Surfaces, *Inzh.–Fiz. Zh.*, 1998, vol. 71, no. 6, p. 1092.

4. Ul'ev, L.M., Slow Flow between Coaxial Conical Surfaces, *Vestn. Kharkov. Politekh. Univ., Mekh. Mashinostroenie*, 1997, issue 7, part 2, p. 2.
5. Ul'ev, L.M., Heat Exchange during a Slow Flow of a Liquid between Coaxial Conical Surfaces, *Teor. Osn. Khim. Tekhnol.*, 2000, vol. 34, no.1, p. 16.
6. Ul'ev, L.M., Nonisothermal Flow of Thermoplastic Polymer Melts in Conical–Cylindrical Spinnerets, *Teor. Osn. Khim. Tekhnol.*, 1996, vol. 30, no. 6, p. 583.
7. Ponomarenko, V.G., Potebnya, G.F., Ul'ev, L.M., *et al.*, Study of the Rheological Properties of High-Viscosity Liquids by Means of an Automated Capillary Viscosimeter, *Inzh.–Fiz. Zh.*, 1990, vol. 59, no. 1, p. 158.
8. Tadmor, Z. and Gogos, C.G., *Principles of Polymer Processing*, New York: Wiley, 1979. Translated under the title *Teoreticheskie osnovy pererabotki polimerov*, Moscow: Khimiya, 1984.
9. Gol'din, A.M. and Karamzin, V.A., *Gidrodinamicheskie osnovy protsessov tonkosloinogo separirovaniya* (Hydrodynamic Foundations of Thin-Layer Separation), Moscow: Agropromizdat, 1985, p. 264.
10. Lykov, A.V., *Teplomassoobmen* (Heat and Mass Transfer), Moscow: Energiya, 1972, p. 560.
11. Ladyzhenskaya, O.A., *Kraevye zadachi matematicheskoi fiziki* (Boundary Problems in Mathematical Physics), Moscow: Nauka, 1973, p. 408.

SPELL: outer@wall
– коэффициент теплоотдачи на границе $\chi = 0$, $\chi = 1$ соответственно, Вт/(м^2 K)
– функция усечения,
confluent